Advances in Water Resources 66 (2014) 32–42

Contents lists available at ScienceDirect

Advances in Water Resources

journal homepage: www.elsevier.com/locate/advwatres

Tree root systems competing for soil moisture in a 3D soil–plant model

Gabriele Manoli [a,b,*], Sara Bonetti [b], Jean-Christophe Domec [c,d], Mario Putti [a], Gabriel Katul [b], Marco Marani [b,e]

[a] Department of Mathematics, University of Padova, Via Trieste 63, 35121 Padova, Italy
[b] Nicholas School of the Environment, Duke University, Durham, NC 27708, USA
[c] Department of Forestry and Environmental Resources, North Carolina State University, Raleigh, NC 27695, USA
[d] Bordeaux Sciences Agro UMR 1391 INRA-ISPA, University of Bordeaux, 33175 Gradignan, France
[e] Department of Civil, Architectural and Environmental Engineering, University of Padova, via Loredan 20, 35131 Padova, Italy

ARTICLE INFO

Article history:
Received 23 September 2013
Received in revised form 27 January 2014
Accepted 28 January 2014
Available online 12 February 2014

Keywords:
Ecohydrology
Numerical modeling
Optimal leaf conductance
Photosynthesis
Root water uptake
Trees competition

ABSTRACT

Competition for water among multiple tree rooting systems is investigated using a soil–plant model that accounts for soil moisture dynamics and root water uptake (RWU), whole plant transpiration, and leaf-level photosynthesis. The model is based on a numerical solution to the 3D Richards equation modified to account for a 3D RWU, trunk xylem, and stomatal conductances. The stomatal conductance is determined by combining a conventional biochemical demand formulation for photosynthesis with an optimization hypothesis that selects stomatal aperture so as to maximize carbon gain for a given water loss. Model results compare well with measurements of soil moisture throughout the rooting zone, of total sap flow in the trunk xylem, as well as of leaf water potential collected in a Loblolly pine forest. The model is then used to diagnose plant responses to water stress in the presence of competing rooting systems. Unsurprisingly, the overlap between rooting zones is shown to enhance soil drying. However, the 3D spatial model yielded transpiration-bulk root-zone soil moisture relations that do not deviate appreciably from their proto-typical form commonly assumed in lumped eco-hydrological models. The increased overlap among rooting systems primarily alters the timing at which the point of incipient soil moisture stress is reached by the entire soil–plant system.

1. Introduction

Background: Forest ecosystems provide many economic, ecological and social benefits [1] and play a key role in regulating the energy, carbon, and water fluxes between the biosphere and the atmosphere. Soil water is extracted by plant roots, flows through the plant vascular system and evaporates from the plant leaves thus providing a bridge in which soil water reservoir and atmospheric water vapor concentration interact. Root water uptake (RWU) controls the water dynamics in the subsurface, thereby affecting plant water availability [2], soil water content [3], and the partitioning of net radiation into latent and sensible heat fluxes thereby impacting atmospheric boundary layer dynamics [1,4,5]. Yet, despite its documented importance, a number of thorny issues remain when representing RWU in hydrological and atmospheric models [6], and addressing a subset of these issues frames the compass of this work. Among the least studied of these issues is the representation of RWU when competition among trees for available root-water occurs. Such competition is rarely accounted for in conventional ecological and hydrological models. Earlier work mostly focused on grass-trees competition in the vertical dimension. In this type of competition, it was assumed that deep tree roots use water not consumed by the shallow grass rooting system [7,8] and the competition for RWU becomes apparent when vertically-averaging the grass-tree rooting system [7,9]. Even within this restricted representation, resolving such rooting competition was shown to be essential in reproducing biomass dynamics [7,9]. One of the barriers to progressing on the root-water competition issue is the inherent three-dimensional nature of the problem. Here, a new 3D model of RWU is developed to investigate the effects of overlapping root-systems within a forest canopy so as to infer up-scaled representation of such competition effects on bulk ecohydrologic models.

RWU modeling: Modeling RWU requires coupling plant transpiration and photosynthesis together with a three-dimensional evolving soil moisture field. Two main approaches, both based on Richards' equation to describe soil water dynamics [2], have been used to model RWU: (1) a macroscopic approach and (2) a

* Corresponding author at: Department of Mathematics, University of Padova, Via Trieste 63, 35121 Padova, Italy. Tel.: +39 049 8271334.
E-mail address: manoli@dmsa.unipd.it (G. Manoli).

http://dx.doi.org/10.1016/j.advwatres.2014.01.006
0309-1708/

microscopic approach that accounts for the detailed root architecture. The first approach accounts for RWU by introducing a "macroscopic" sink term, generally defined as a function of spatially-distributed root parameters (e.g., root length density). This approach assumes that the vertically integrated RWU can be represented via a potential transpiration dictated by atmospheric demand for water vapor modulated by an ad hoc water stress function (e.g., Feddes approach [10]). Some compensatory mechanisms have been incorporated within such a framework [11,12]. When water potential gradients (WPG) are employed, this approach can reproduce important processes such as hydraulic redistribution (HR) [13]. HR has been observed in a number of experiments [14,15] and included in different modeling approaches [13,16–22]. While most models in this class can satisfactorily reproduce both compensation and redistribution mechanisms, they generally use a vertically distributed RWU approximation, thereby censoring any horizontal interactions among plants. Multidimensional macroscopic models do exist [12,23], but they generally use simplified RWU functions that may be unrealistic in heterogeneous soils [24]. The importance of a three-dimensional perspective has been recently underlined [25] spawning a number of simulations of water flow through soil and roots using a root hydraulic network [2,25–27]. This second approach includes detailed plant-scale models based on explicitly resolved root architecture coupled with the three-dimensional Richards equation for water flow in the soil-root system of an isolated single small plant or seedling [2,25,26]. Because the precise root architecture for multiple interacting trees is rarely known a priori, and given the computational burden involved, a root architecture approach is not yet feasible for large scale hydrological simulations. An intermediate approach that retains the 3D properties of the problem and yet provides a numerically-viable simplified RWU approach is needed when exploring the interplay of hydrological, physiological, and ecological mechanisms at the watershed scale. Existing 3D models (belonging to both categories) commonly neglect photosynthetic processes, which largely controls transpiration, and hence RWU. An approach that also accommodates these mechanisms and can be embedded in a robust three-dimensional soil moisture model offers a decisive advantage when generalizing plant-water relations at larger scales. With such a representation, the competition between plants for soil water (e.g., neighboring trees in a forest stand) can be made explicit and its effects on upscaled watershed processes can be explored.

Objectives: The main objective here is to develop a mechanistic 3D model of RWU so as to explore the implications of root competition on ecosystem transpiration and carbon uptake. More specific objectives are to (1) develop and apply a soil–plant-atmosphere model incorporating a 3D description of soil water dynamics, (2) investigate the effects of some biotic and abiotic compensatory mechanisms such as HR and Darcian redistribution on RWU and water use efficiency, and (3) evaluate the effects of tree-to-tree overlapping root zones on ecosystem level RWU rates. The main novelty is a framework in which a 3D hydrological model is coupled to plant transpiration and leaf photosynthesis that is then used to explore root water uptake for overlapping tree rooting systems in the presence of dynamic groundwater fluctuations.

2. Mathematical model

The transpiration flux is expressed in terms of gradients in water potential through a series of conductances along the pathway connecting water from the soil (ψ_i), to the xylem (ψ_R), and to the leaf (ψ_L) (Fig. 1). Stomatal conductance is assumed to maximize carbon gain, while minimizing water loss. The following assumptions are made [22]:

(a1) water extracted by roots only feeds transpiration and no water storage occurs within the plant system,
(a2) each soil layer is directly linked to the xylem through the root biomass allocated to the same layer,
(a3) energy losses in the root system are negligible compared to the dissipation in the soil and soil-root interface,
(a4) RWU is not limited by any other mechanism (e.g., nutrient limitation),
(a5) root growth is here ignored, though it may be significant at long time scales.

2.1. Soil–plant exchanges

A recent 1D root model [22] is expanded here to a 3D general framework. Richards' equation is used to describe soil moisture dynamics in a three-dimensional porous medium and is given as:

$$S_s S_w(\psi)\frac{\partial \psi}{\partial t} + n\frac{\partial S_w(\psi)}{\partial t} = \vec{\nabla}\cdot\left[\mathbf{K}_s K_r(\psi)\left(\vec{\nabla}\psi + \eta_z\right)\right] + q(\psi, x, y, z, t, \psi_L), \quad (1)$$

where S_s is the elastic storage term (m^{-1}), S_w is water saturation (–), ψ is the soil water potential (m), t is time (s), n is the porosity (–), $\mathbf{K}_s$ is the saturated hydraulic conductivity ($m\ s^{-1}$) tensor, K_r is the relative hydraulic conductivity (–), $\eta_z = (0,0,1)^T$ is the gravitational potential energy gradient with z, the vertical coordinate, directed upward and $q(\psi, x, y, z, t, \psi_L)$ is a macroscopic source/sink term (s^{-1}) through which soil water dynamics is coupled with the root–plant system via the leaf water potential ψ_L. Anisotropic saturated hydraulic conductivity is modeled as a diagonal matrix with diagonal elements K_x, K_y, and K_z, the saturated hydraulic conductivities along the coordinate directions. Eq. (1) is highly nonlinear due to the functional dependence upon pressure head of the soil water retention curves, which are modeled following van Genuchten and Nielsen [28]. The numerical solution to Eq. (1) is obtained by means of a Finite Element approach with linear (P1) basis functions and implicit Euler time-stepping, as implemented in the CATHY model [29]. The scheme considers nonlinear boundary conditions at the soil surface to account for ponding or evaporation limitations due to variable surface soil moisture. The numerical solver is based on an unstructured tetrahedral grid and employs time step adaptation to ensure convergence for highly nonlinear problems and address the ODE stiffness resulting from the discretization of the nonlinear source term. Inexact Krylov-based Picard iteration with ad hoc efficient preconditioning is used in the solution of the nonlinear system of equations [30–32]. Discretization of the source term is obtained by means of the second order accurate midpoint rule, by which at each grid node i the source term $q_i = q(\psi_i, x_i, y_i, z_i, t, \psi_L)$ is multiplied by the corresponding nodal soil volume V_i. Coupling between the soil and the root system proceeds as follows: Single plants are defined by a surface grid node, j (with j between 1 and the number of plants in the model domain), which can be identified as the base of the plant trunk. The total water uptake per unit soil volume from node i, appearing in Eq. (1), is expressed as the uptake from all plants having non-zero root biomass at node i, i.e., $q_i = \sum_j q_{ij}$. The term q_{ij} is the soil water uptaken (per unit soil volume) by the roots of plant j at grid node i. A plant node j is connected to each soil node within its root zone through a conductance, g_{ij}, representing the path traveled by water from the soil pores into the nearest root within the finite element centered in i. The conductance g_{ij} expresses the water flux from the soil to the root (or viceversa) crossing the root membrane per unit area of the membrane and per unit difference of the total water potential between the soil and the root (see inset in Fig. 1). To obtain the flux per unit soil volume of the domain entering (or exiting) the root system at node i, it is necessary to account for the total root surface area per unit soil volume,

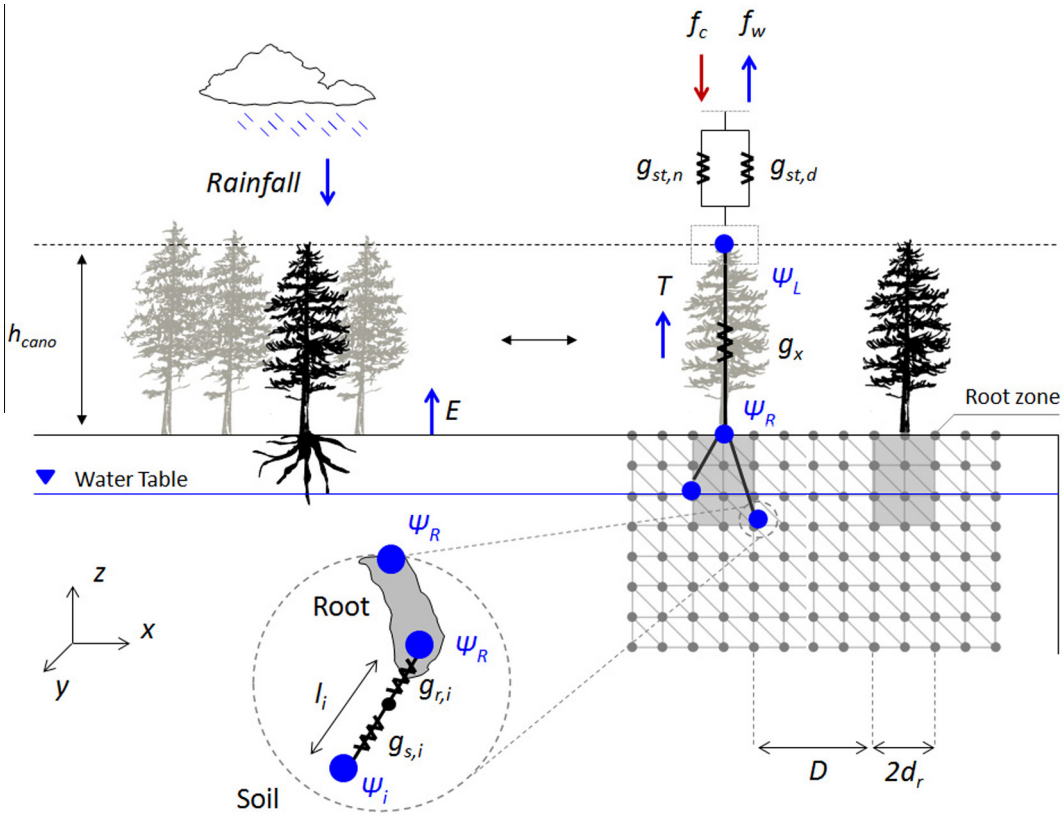

Fig. 1. Model structure: the pathway of water movement from the soil through the plant system into the atmosphere modeled using a series of conductances. Water fluxes are proportional to potential energy gradients between the soil (ψ_i), the root system (ψ_R), and the leaves (ψ_L). Rainfall, soil evaporation and water table fluctuations are specified as boundary conditions and the root water competition between neighboring trees is evaluated by changing the spacing D between two identical pine trees, each having a root zone length d_r.

$a_{R,i}$ [$m^2_{root}\ m^{-3}_{soil}$], such that the soil water (per unit soil volume) uptaken by the roots of plant j at grid node i is:

$$q_{i,j} = -g_{i,j}\left[(\psi_{R,j} + z_{R,j}) - (\psi_i + z_i)\right] a_{R,i}. \tag{2}$$

The total root surface area per unit soil volume is computed as $a_{R,i} = 2\pi r B_i$, where the effective root radius r is assumed to be 2 mm and B_i is the root length density at node i ($m_{root}\ m^{-3}_{soil}$); $z_{R,j}$ is the elevation of the base of the trunk and z_i is the elevation of the ith grid node (m). Because of Assumption 3 above, the hydraulic head is everywhere constant within the root system set to $\psi_{R,j} + z_{R,j}$, which appears in Eq. (2) irrespective of the specific node i considered (see Fig. 1). The total soil-to-root conductance, $g_{i,j}$, is calculated by considering the effect of soil conductance ($g_{s,i}$), relative to the average path traveled by water from the soil to the nearest root, and of the root membrane conductance ($g_{r,i}$). The conductance of the path traveled within the soil to the nearest root is $g_{s,i} = K_i l_i^{-1}$, where $K_i = \|K_s K_r\|_i$ is the norm of the soil hydraulic conductivity ($m\ s^{-1}$) evaluated at node i and l_i the rizhosphere radius (m), i.e., the mean length traveled from the bulk soil to the root surface. The length l_i can be estimated as $l_i = \alpha/\sqrt{\pi B_i}$, where $\alpha = 0.53$ is an empirical coefficient [13,33]. The effective conductance (not conductivity) resulting from two conductances in series is given by $g_{i,j} = (g_{s,i} \cdot g_{r,i})/(g_{s,i} + g_{r,i})$ [22].

The sign of $q_{i,j}$ is controlled by the energy gradient between the soil and the plant xylem and it defines the direction of water flow at the soil–plant interface: when $\psi_{R,j} + z_{R,j} < \psi_i + z_i$, soil water is uptaken by the root system (RWU), otherwise water is redistributed by roots into the soil (HR). As a consequence of RWU, energy gradients originate in the soil, thus activating another compensatory mechanism: Darcian redistribution. The Darcy's flux is controlled by the soil parameters only and it is computed here as the residual between q_i and the left term of Eq. (1).

The transpiration rate T_j ($m^3\ s^{-1}$) of plant J is driven by the potential energy gradient between the trunk base and the leaf [22]:

$$T_j = -g_{x,j}\left[(\psi_{L,j} + z_{L,j}) - (\psi_{R,j} + z_{R,j})\right] A_{x,j}, \tag{3}$$

where $\psi_{L,j}$ is the leaf water potential (discussed later), $g_{x,j}$ is the xylem conductance, $A_{x,j}$ is the xylem cross sectional area (m^2), and $z_{L,j}$ is the elevation at which the effective leaf water potential is evaluated at (m). The conductance $g_{x,j}$ accounts for the vulnerability of the xylem to cavitation according to Daly et al. [34] (see Supplementary material for details). The pressure head in the xylem, $\psi_{R,j}$, is now determined by equating the transpiration rate T_j to the total water flux uptaken by the root system of plant j, i.e., $T_j = \sum_i q_{i,j} \cdot V_i$. This equality yields [22]:

$$\psi_{R,j} = \frac{g_{x,j} A_{x,j} (\psi_{L,j} + h_{c,j}) + S1_j}{S2_j + g_{x,j} A_{x,j}}, \tag{4}$$

where $h_{c,j} = z_{L,j} - z_{R,j}$ is the canopy height, $S1_j = \sum_i g_{i,j} a_{R,i} (\psi_i - d_{i,j}) V_i$, $d_{i,j}$ being the difference in elevation between the ith soil node and the base of the trunk, and $S2_j = \sum_i g_{i,j} a_{R,i} V_i$. The leaf water potential $\psi_{L,j}$ is unknown and, due to the dependence of the sink term $q_{i,j}$ on $\psi_{L,j}$, Eq. (1) is under-constrained. A leaf scale mass transfer model is now needed to mathematically close the problem.

2.2. Plant-atmosphere

Even though a single $\psi_{L,j}(t)$ is used to represent the water potential in the entire canopy, the model here incorporates a

vertically-explicit description of the light regime. This description decomposes the leaf area into vertical layers so as to account for light attenuation and its effects on the photosynthesis calculations [22]. At each canopy layer, the leaf-scale transpiration is defined by the mass transfer of water vapor between the leaf and the atmosphere at the canopy layer r:

$$f_{w,j,r}(\psi_{L,j}) = a\, g_{st,j,r}(\psi_{L,j})\mathrm{VPD}\,\epsilon_w \tag{5}$$

where $a = 1.6$ is the relative diffusivity of water vapor with respect to CO_2, $g_{st,j,r}$ is the CO_2 stomatal conductance at canopy layer r (mmol m^{-2} s^{-1}), VPD is the vapor pressure deficit (assuming that the leaf is well coupled to the atmosphere) and $\epsilon_w = \mathrm{MW}_w/\rho_w$, where MW_w (g mol^{-1}) and ρ_w (kg m^{-1}) are molar weight and density of water, respectively. The *VPD* is computed as the difference between vapor pressure at saturation and ambient conditions [22]. Here, air temperature, water vapor and CO_2 concentrations are assumed to be vertically uniform within canopy air volume set to their (time-varying) measured values above the canopy and only the light regime is determined at different canopy layers. The leaf photosynthesis at canopy layer r is described by a biochemical demand function [35]:

$$f_{c,j,r} = \frac{a_{1,r}}{a_2 + c_{ic,r}}\left(c_{ic,r} - c_{cp}\right), \tag{6}$$

where the photosynthetic parameters a_1 and a_2 are selected depending on whether light or Rubisco limits photosynthesis [22] at layer r, c_{cp} is the CO_2 compensation point [mmol μmol^{-1}]. The inter-cellular CO_2 concentration c_{ic} can be eliminated and replaced by stomatal conductance when assuming Fickian mass transfer between the leaf and the atmosphere [22] governs CO_2 exchange. When Rubisco is limiting $a_1 = V_{c,\max}$ and $a_2 = K_c(1 + \frac{C_{o,a}}{K_o})$ where $V_{c,\max}$ is the maximum carboxylation capacity referenced at 25 °C, K_c and K_o are the Michaelis constants for, respectively, CO_2 and O_2 fixation at 25 °C and $C_{o,a}$ is the oxygen concentration in the atmosphere. When light is the limiting factor, $a_1 = \gamma Q_{p,r}$ and $a_2 = 2c_{cp}$, where γ is the apparent quantum yield (–), $Q_{p,r}$ is the photosynthetically active radiation at the canopy layer r ($\mu mol\ m^{-2}$ - s^{-1}). Light attenuation within the canopy is modeled using an extinction coefficient accounting for leaf angle distribution and solar zenith angle [22]. The photosynthetic parameters are adjusted for air temperature as described elsewhere [36]. Stomatal conductance is optimized for maximum carbon gain according to a linearized formulation also described elsewhere [22,37]. Because nocturnal transpiration can be significant [13,20,38], the leaf-level formulation [37] is modified to include nighttime transpiration. This modification is based on the fact that effective bulk leaf conductance $g_{st,j}$ accounts for both - the optimal stomatal control by the plant on the stomatal aperture, encoded in $g_{st,d}$, and a residual loss $g_{st,n}$ when stomata are almost closed (e.g., leaks due to imperfect closure, curticular, etc.…). Under the assumption that these pathways are parallel (Fig. 1), it follows that $g_{st} = g_{st,d} + g_{st,n}$. As conventional in stomatal optimization theories [37], an objective function for the plant is assumed to be maximizing the leaf carbon gain f_c at a given water loss f_w (in units of carbon) for a species-specific water use efficiency λ. The following objective function can thus be defined: $f(g_s) = f_c - \lambda \cdot f_w$. Assuming that leaves optimally and autonomously regulates $g_{st,d}$ only, it is possible to set $\partial f(g_{st})/\partial g_{st,d} = 0$ and solve for $g_{st,d}$. Hence, it follows that at the canopy layer r [37]:

$$g_{st,r}(\psi_L) = \frac{a_{1,r}}{a_2 + s\ c_a}\left[-1 + \left(\frac{c_a}{a\ \lambda(\psi_L)\ \mathrm{VPD}}\right)^{1/2}\right] + g_{st,n}, \tag{7}$$

where s is a model constant connected to the long-term c_i/c_a, c_a [mmol mol^{-1}] is the CO_2 concentration in the atmosphere and the cost parameter λ [$\mu mol\ mol^{-1}$], i.e., the cost of water for the plant to complete the photosynthesis, is estimated from the time-integrated leaf water potential according to Manzoni et al. [39]. We refer to [22,37] for further details on the optimality model. The nocturnal stomatal conductance $g_{st,n}$ can be determined from the relation between sapflow and VPD [20]. Since the cost parameter varies over much longer time scales than the leaf potential (e.g., daily), a single value of λ is used for the different canopy layers (but time varying) and the center of the canopy is used in the calculations of $\psi_{L,j}(t)$ [22].

2.3. Non-linear closure equation

Because of the flux continuity across the soil–plant system, integrating Eq. (5) over the leaf area and equating to Eq. (3) leads to the following nonlinear closure equation for plant j:

$$G_j(\psi, \psi_{L,j}) = T_j(\psi, \psi_{L,j}) - \sum_r f_{w,j,r}(\psi_{L,j}) \cdot LAI_{j,r} \cdot A_{c,j} = 0, \tag{8}$$

where $A_{c,j}$ is the canopy projected area (m^2) and $LAI_{j,r}$ is the leaf area index at the canopy layer r ($m^2_{\mathrm{leaf}}\, m^{-2}_{\mathrm{soil}}$). Eq. (1) is defined for every plant j and is coupled to the discretized Richards equation to augment the nonlinear system for the variable $\psi_{L,j}$. Because of the presence of several inflection points in G_j, the numerical solution is obtained by the secant method at every Picard iteration. Let m be the external Picard iteration counter and k the time step index, the value of $\psi_{L,j}$ is obtained by the following internal iteration on n:

$$\psi^{n+1}_{L,j} = \psi^{n}_{L,j} - G_j\left(\psi^{k+1,m}, \psi^{n}_{L,j}\right)\frac{\psi^{n}_{L,j} - \psi^{n-1}_{L,j}}{G_j\left(\psi^{k+1,m}, \psi^{n}_{L,j}\right) - G_j\left(\psi^{k+1,m}, \psi^{n-1}_{L,j}\right)}.$$

The initial guesses $\psi^0_{L,j}$ and $\psi^1_{L,j}$ are evaluated within the range of physical values for the leaf water potential (here we assumed $-10 \leqslant \psi_{L,j} \leqslant 0$ MPa and we used the boundaries of the interval as initial guesses) using a few bisection steps to ensure the existence of a root of G_j, i.e., $G_j(\psi^{k,m}, \psi^0_{L,j})G_j(\psi^{k,m}, \psi^1_{L,j}) < 0$. When no roots exist, the value of $\psi_{L,j}$ that minimizes G_j is assumed as the solution.

3. Case study: a Loblolly pine plantation

3.1. Site description

The model is evaluated using a 2-year data set collected in a Loblolly pine plantation situated in the lower coastal plain of North Carolina, USA (35°11′N, 76°11′W). A description of the study area and data collected can be found elsewhere [40,20]. Briefly, the plantation (denoted as US-NC2 in the Ameriflux database) is a 100 ha mid-rotation Loblolly pine stand established in 1992 after clear cutting the mature pine trees [20]. The trees were planted at a 1.5 m × 4.5 m spacing [40]. The plantation is drained by a network of parallel ditches (90–130 cm deep; 90 m spacing) and more widely spaced roadside canals. The meteorological, hydrological, and eco-physiological data used were collected during years 2007 and 2008. Input micro-meteorological data (e.g., air temperature, photosynthetically active radiation or PAR, relative humidity, rainfall) were recorded every minute and averaged every 30-min. Water vapor fluxes were also measured using an eddy covariance (EC) system located on the meteorological tower at the site [40]. The EC system sampling frequency is 10 Hz and the averaging period is 30 min, synchronized with the meteorological measurements. The soil is stratified as a sequence of an organic horizon about 30 cm deep, followed by a 30 cm thick organic-sandy layer and by a sandy-loam layer below 60 cm [20,40,41]. The soil hydraulic parameters are described elsewhere [41] and summarized in Table 1. Soil moisture was measured continuously at 10, 20, 30, 40, 50, 60, 80, and 140 cm depths using Sentek EnviroSCAN capacitance sensors (Sentek Sensor Technologies,

Table 1
Soil hydraulic parameters: porosity values n are defined according to Domec et al. [20] and the saturated hydraulic conductivities $K_{x,y}$ and K_z are based on laboratory testing from Diggs [41]. The residual soil moisture content θ_r, the capillary or air entry pressure ψ_s [30], and the exponent parameter n_{vg} are the coefficients of the soil water retention curves according to van Genuchten and Nielsen [28] and Paniconi and Putti [30].

Depth (mbs)	n (–)	K_{soil} (m s^{-1})	θ_r (–)	ψ_s (m)	n_{vg} (–)
0.00–0.30	0.50	7.2×10^{-5}	0.03	−0.10	1.43
0.30–0.60	0.45	1.0×10^{-4}	0.02	−0.10	1.33
0.60–5.00	0.37	7.2×10^{-5}	0.03	−0.25	2.50

Stepney, Australia) and water table fluctuations were monitored every hour by a groundwater well installed at the site [40]. Tree transpiration was separately determined from trunk sap flux measurements on different pine trees. Specifically, sapflux measurements were collected at 1.4 m above the ground at four radial positions using 20 mm heat dissipation probes [15]. These transpiration estimates are interpreted as the integrated *RWU* and are used in comparisons with model results. Plant model parameters are based on literature values or assumed according to field observations (e.g., projected canopy area, xylem area and root radius). All the model parameters are illustrated in Table 2.

3.2. Model run setup

The model is first compared with measured transpiration and photosynthesis for a single pine tree by using a 1D vertical domain. These simulations are intended to calibrate the model parameters, ensure a physically plausible model behavior, and provide a reference 1D case (i.e., not including competition among neighboring trees). Given the 3D nature of the model formulation, the dimensionality of the model is reduced to 1D by adopting a model domain that consists of vertical line of nodes, where Richards' equation is solved for, surrounded by nodes where boundary conditions (BCs) are imposed using measured water table levels. The 1D model thus reproduces an equivalent soil column of diameter $2d_r$ (see Fig. 1). The vertical profile of the root length density B_i is based on Domec et al. [20], where measurements commenced at 0.15 m below the soil surface. The B_i near the surface was determined by extrapolation using a typical exponential root distribution profile [22]. Field measurements of the meteorological and hydrological drivers (e.g., rainfall, temperature, relative humidity, PAR, etc.) are used to calculate the atmospheric forcing. Rainfall data are corrected for canopy interception assuming an interception rate of 15% [40]. An understory EvapoTranspiration (ET) is calculated as the difference between the EC measured latent heat flux (LE) above the canopy converted into mass units [40] and the sap flow data. The resulting net flux is then imposed as a Neumann boundary condition at the soil surface of the model domain. Input precipitation is considered as a potential rate and actual infiltration is evaluated based on the soil current saturation state, allowing switching between Neumann and Dirichlet BCs in case of water ponding [29].

The model is subsequently used to simulate two identical and interacting Loblolly pine trees under conditions similar to those observed within the plantation (3D simulations). Considering the tree spacing at the site, a 10 m × 5 m × 5 m model domain is used to represent a portion of the plantation thereby avoiding boundary effects on the numerical solution. The effect of tree competition for RWU is investigated by simulating a 100 days drying cycle. The atmospheric forcing recorded on July 14th, 2007 (a typical day characterized by high transpiration thereby highlighting the implications of root competition on soil water availability and RWU), are repeated periodically during the simulated dry down period: the water table was kept constant at 3 m below the surface and no-flow conditions were imposed on the outer soil boundary. Simulations with different tree spacing D, defined as the distance between the root systems (such that $D < 0$ indicates partially overlapping root systems), are also explored (Fig. 1).

In all the 3D model calculations, the following assumptions are adopted and repeated here for clarity: (a) the root system is static (root growth is neglected) and (b) only competition for water is considered, assuming that trees do not compete for other resources. While competition for light is another major factor in forested canopies, the outcome of this competition is not explicitly considered here though it does affect canopy height, leaf area, and ratio of leaf-area to root-area index that are pre-specified here. To compress the 3D simulations so that they are comparable with the 1D simulation results, the root distribution is assumed constant in the horizontal directions and the same volume of roots as in the 1D simulations is considered. Preliminary simulations of

Table 2
Plant model parameters: values are based on previous literature or on field measurements.

Parameter	Description	Units	Values	References
Plant parameters				
h_{cano}	Plant/canopy height	m	17	[20]
A_{cano}	Projected canopy area	m^2	9	Assumed
A_{xylem}	Xylem area	m^2	0.06	Assumed
r	Root radius	m	0.02	Assumed
RAI	Root area index	m^2 m^{-2}	2.1–4.7	[20]
g_r	Root conductance	s^{-1}	3×10^{-11}	Assumed
B	Root length density	cm cm^{-3}	0.07–3.70	[20]
LAI	Leaf area index	m^2 m^{-2}	2.5–5.6	[20]
Xylem conductance				
$g_{x,max}$	Maximum xylem conductance	s^{-1}	5×10^{-6}	Assumed
d	Vulnerability curve coefficient	m	200	[22,42]
c	Vulnerability curve coefficient	–	2	[22,42]
Photosynthetic model				
$V_{c,max25}$	Maximum carboxylation capacity at 25 °C	μmol m^{-2} s^{-1}	41	[20]
$K_{c,max25}$	Michaelis constant for CO_2 fixation at 25 °C	μmol mol^{-1}	300	[22]
$K_{o,max25}$	Michaelis constant for O_2 fixation at 25 °C	mmol mol^{-1}	300	[22]
$c_{p,25}$	CO_2 compensation point at 25 °C	mmol μmol^{-1}	2.6	[22]
Stomatal optimality model				
λ^*_{max}	Maximum marginal water use efficiency	μmol mol^{-1}	1755	[39]
β	Empirical parameter	m^{-2}	1.2×10^{-5}	[39]
$\psi_{L,max}$	Leaf water potential at maximum λ	m	−277	[39]
γ	Apparent quantum yield	–	0.015	[43]
a	Relative H_2O/CO_2 diffusivity	–	1.6	[37,22]
s	Coefficient for g_s calculation	–	0.7	[37,22]
$C_{o,a}$	O_2 concentration in air	mmol mol^{-1}	210	[37,22]
c^*_a	Reference CO_2 concentration	μmol mol^{-1}	400	[37,22]
c_a	Ambient CO_2 concentration	mmol mol^{-1}	380	[37,22]
$g_{s,n}$	Nocturnal stomatal conductance	mmol m^{-2} s^{-1}	18	[20]

a drying cycle were run both with the 1D and 3D set up and comparable results were obtained (not shown here for brevity). A homogeneous lateral root distribution was not based on field conditions, but it is the simplest assumption that allows addressing differences in soil water dynamics and transpiration responses when comparing the 1D and 3D setups.

4. Results and discussions

4.1. Model calibration

A comparison between measured and modeled soil moisture is presented in Fig. 2 for the entire year of 2007. The model satisfactorily captures the observed soil moisture patterns at all depths. The initial discrepancy between simulations and measurements is attributed to the choice of the initial pressure distribution (hydrostatic profile based on the observed water table), but the discrepancy between the model system state, forcings, and measurements is greatly reduced after just a few rainfall events. Other discrepancies between model results and measurements are related to the occasional rapid transients in soil moisture within the deeper layers. These measured transients can be plausibly explained by small scale heterogeneities not accounted for in the model (e.g., preferential flow paths causing fast downward flow or presence of sand/clay lenses not included here). Some evidence that these small scale heterogeneities play a role can indeed be fingerprinted. For example, the peak in soil moisture observed at 1 m below the soil surface on day 305 (Fig. 2d) can be explained by the presence of preferential flows since this peak is not related to a water table fluctuation and is not observed in the upper soil layers (Fig. 2a–c). Despite these deviations between model calculations and measurements, it can be surmised that the calibrated model behavior realistically reproduces the main processes impacting soil moisture dynamics in this system.

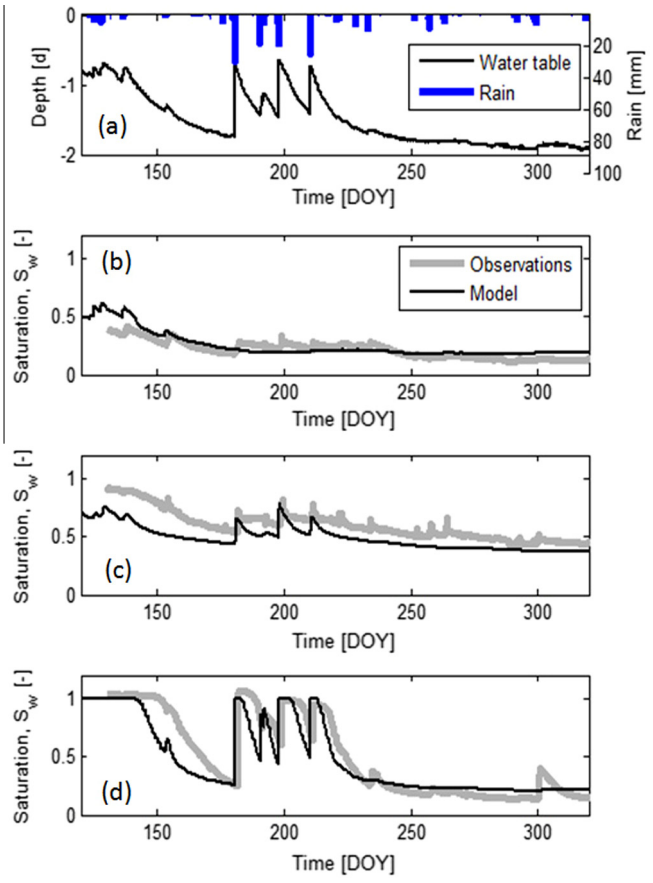

Fig. 2. Soil water dynamics: (a) rainfall events and water table fluctuations observed at the site during year 2007. Model results are compared with soil saturation S_w measured at a depth of (b) 10 cm, (c) 50 cm and (d) 100 cm.

The ability of the model to describe the RWU mechanisms are shown in Fig. 3. The model captures the biotic behavior in terms of leaf water potential (Fig. 3b) and transpiration (Fig. 3c and d). Because of the single-layer approximation for the above-ground leaf pressure, modeled ψ_L is compared with measurements from both leaf and branches, showing a reasonable match with branch values. The measured sap-flux (Fig. 3c) also shows large variability among different trees, but the model provides an adequate description of the mean behaviour (Fig. 3c). The dynamics of RWU along the soil column (of diameter $2d_r$ as identified in Fig. 1) during the two-years period is also illustrated in Fig. 4b. The RWU is higher during the summer periods as expected and it decreases during the winter despite the ever-green nature of this stand and the warm climate. During dry periods, soil water is first redistributed by roots in the top soil, subsequently redistribution is more prominent in the deeper layers (Fig. 4d). In particular, HR is not high during the first year, as the water table is shallow, while it increases during the second year, due to a significant drop in the water table (Fig. 4d). The range of variability of HR spans two orders of magnitude across ecosystems [21] and, as discussed elsewhere [15], it can mitigate the effects of soil drying on stand evapotranspiration and net primary productivity. In Loblolly pine plantations, reported estimates of HR can exceed 1 mm d^{-1}, ranging between 6% and 12% of daily transpiration [15]. The model here predicts a peak HR rate of 0.5 mm d^{-1} in 2007 and 1.1 mm d^{-1} in 2008 (i.e., 10–20% of daily transpiration), in agreement with the magnitude of HR observed at the site [20] and reported elsewhere in the literature [21].

4.2. Trees competition

Having demonstrated the model skills, a system of two identical trees (T1 and T2) with interacting roots is now considered so as to explore the effect of root competition on RWU and photosynthesis during a 100 day drying cycle. Each tree has a rooting system with a projected area of 9 m^2 (i.e., $d_r = 1.5$ m, see Fig. 1), assuming a linear relation between canopy and roots projected area. Configurations ranging from no interaction ($D = 1.0$ m) to progressively greater overlap ($D = -0.5$ m and $D = -1.5$ m, corresponding to overlaps of 17% and 50% of the projected area of a single root system) are now examined. In the overlap areas, the total RWU increases due to increased local root biomass (Fig. 5). An increased root overlap leads to an RWU vertical distribution that appears less localized within the root zone when compared to the biomass proportion allocated to each layer (the 'bumps' in Fig. 4a). This reduced spatial localization in RWU away from the root density distribution is due to a proportionally greater uptake in the remaining layers, partly activated by the compensatory mechanisms (HR and Darcian redistribution). When the response of a single tree is considered (e.g., T1, as the responses are equal, due to symmetry), greater interaction among the rooting systems causes an earlier onset of HR and of water stress, with a corresponding decrease in RWU (Fig. 6a and b). This also results in a faster decline in leaf water potential and a corresponding increase of the cost parameter λ (Fig. 6c and d), causing rapid censoring of leaf transpiration.

The space–time distributions of water fluxes exchanged by one tree with the soil within its root zone also show some interesting patterns as the interaction between root systems is increased (Fig. 7). As noted earlier, the soil dries more rapidly when root competition for water is intensified, with a corresponding

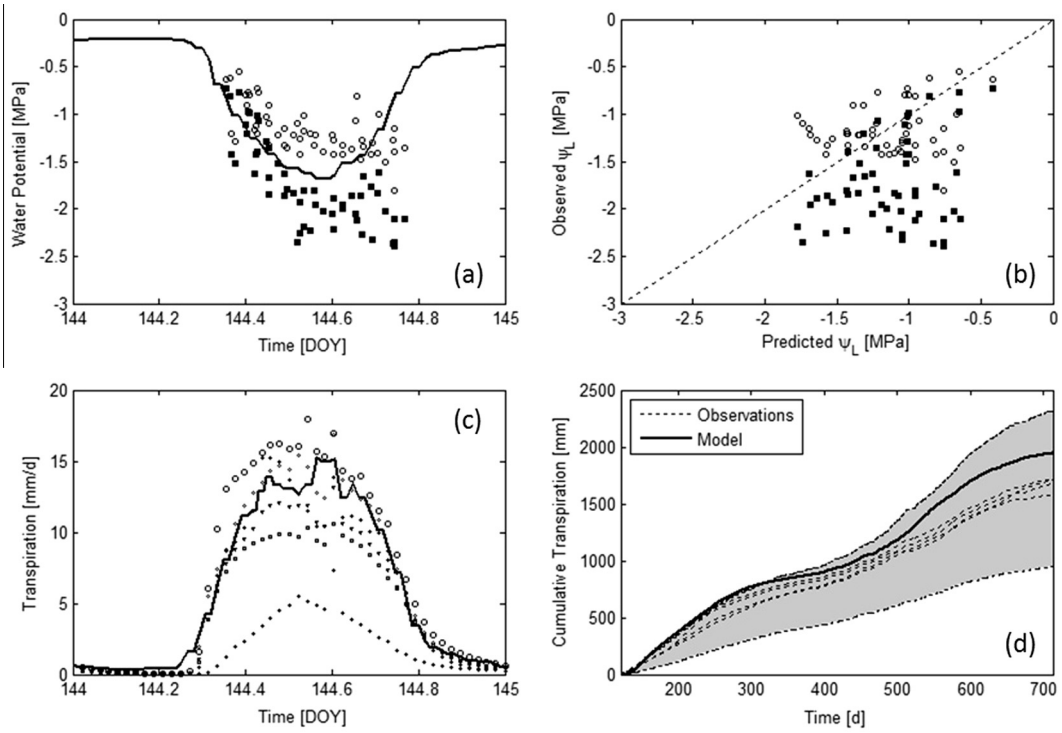

Fig. 3. Tree transpiration dynamics: (a) modeled leaf water potential ψ_L and (c) tree transpiration during an exemplary day (day 144 of year 2007). Leaf (■) and branch (○) water potentials measured on different days of year 2007 are also compared with modeled ψ_L in panel (b) and shown as reference in panel (a). Sap flow measurements from different trees are compared with modeled transpiration on day 144 (different symbols in panel c) and cumulative transpiration over year 2007 and 2008 (dashed lines in panel d).

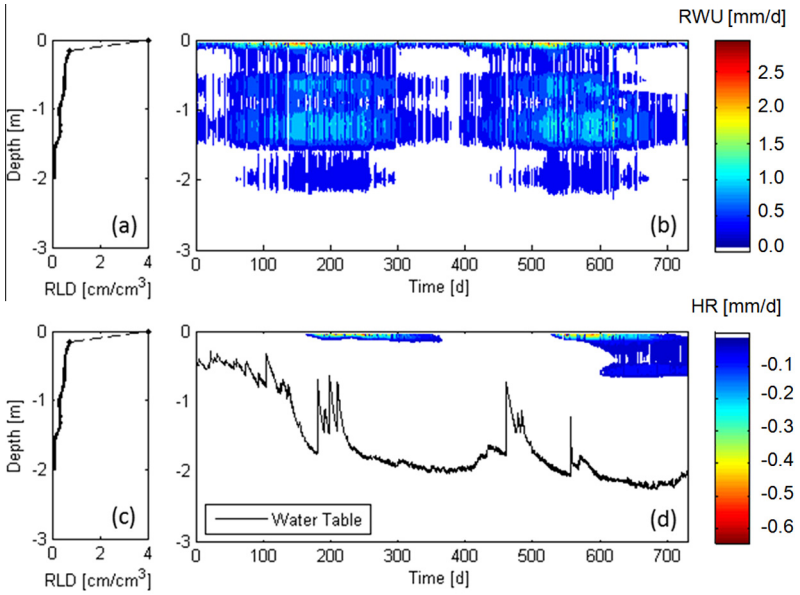

Fig. 4. Observed root density profile (a, c), modeled RWU (b) and HR (d) during year 2007 and 2008 at different soil depths. The water table fluctuations are also shown (black line in panel b).

inhibition of RWU and a faster shift of the active uptake layer to greater depths (Fig. 7a and b). The HR flux initially sustains RWU in the top soil layers (Fig. 7a and b), where redistribution by Darcy's flow is partially inhibited (Fig. 7c and d) by the low soil water saturation and the correspondingly low hydraulic conductivity. Darcian redistribution is, on the contrary, most effective in providing soil moisture within the deeper layers (Fig. 7e and f), where the largest proportion of RWU takes place when most of the soil column has dried down. Overall, RWU is sustained by upward redistribution of water both through the roots (Fig. 7d) and through Darcian flow (Fig. 7e and f) but, as e.g., shown in [22], Darcy's flow accounts for the majority of the redistributed water.

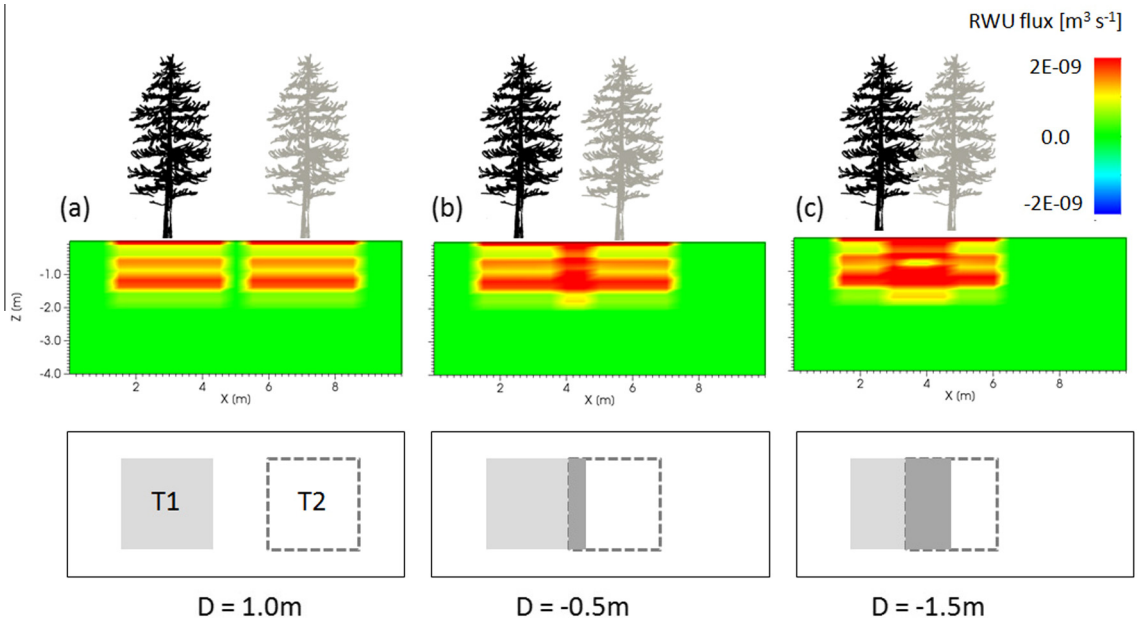

Fig. 5. Simulation results of RWU by multiple trees. The RWU rates at time t = 5.5 days (after the start of the drying experiment) are shown for the test cases with different tree spacing: (a) $D = 1$ m, (b) $D = -0.5$ m, and (c) $D = -1.5$ m.

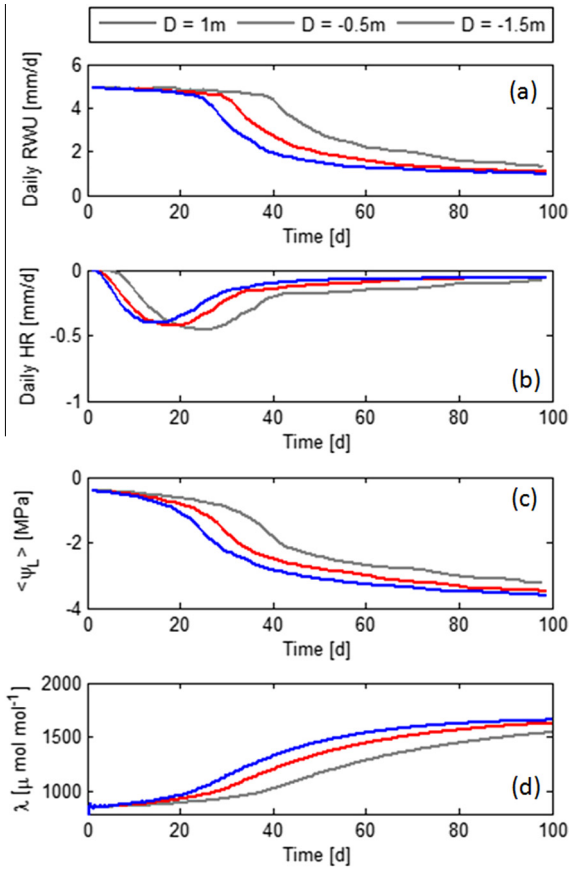

Fig. 6. Transpiration dynamics of tree T1 for different spacings D: (a) daily RWU, (b) HR, (c) daily averaged ψ_l and λ are shown for the case of non-overlapping ($D = 1$ m) and overlapping ($D = -0.5$ m and $D = -1.5$ m) root systems.

Also, it should be emphasized that HR and the Darcian redistribution act in concert within the root zone so as to mediate the spatial regions of reduced soil moisture.

The robustness of these patterns for different root density profiles and soil hydraulic properties have also been explored (results shown in the Supplementary material). Briefly, drying fronts with the same forcings and boundary conditions but with an exponentially distributed root biomass having the same total biomass ($B(z) = e^{a \cdot z + b}$, where a and b are parameters) were simulated. The same numerical experiments were run assuming uniform sand ($K_s = 10^{-4}$ m s^{-1}) or silt ($K_s = 10^{-7}$ m s^{-1}). Collectively, these simulation results robustly show the dominance of Darcian upward redistribution to sustain RWU when compared to root HR. The latter provides significant contribution only near the soil surface, and in the initial phase of the soil drying. When the top soil layer is dry, the hydraulic conductivity there rapidly becomes small thus suppressing further root HR: water potentially lifted by the root system cannot in this case infiltrate into the surrounding soil. A second robust feature is that Darcian redistribution tends to be concentrated in the deeper layers, where a greater mean soil saturation ensures relatively high values of soil hydraulic conductivity and allows significant amounts of water to be moved towards the lower boundary of the root zone. As expected, a more conductive soil (sand) produces a faster transition towards stressed plant conditions, but still induces a significant amount of water redistribution by Darcian flow (in the deeper rooting zone) and by the root system (in the upper layers at the initial stages of the drying experiment). In all cases, root competition more rapidly pushes the system to drier conditions and amplifies the importance of these two redistribution mechanisms to support RWU and carbon assimilation.

4.3. Transpiration and soil saturation

A 'macroscopic' relation between ET and the root-zone averaged saturation, $\bar{S}_w$, is often assumed in bulk ecosystem models seeking to capture the essential components of the soil–plant-atmosphere system [44–48]. Typical bulk models are based on a water balance equation describing the change in soil saturation within the entire root-zone as a function of water infiltration (generally accounting for stochastic rainfall, canopy interception and run-off rates [46–48]) and ET. The ET rate in this context is

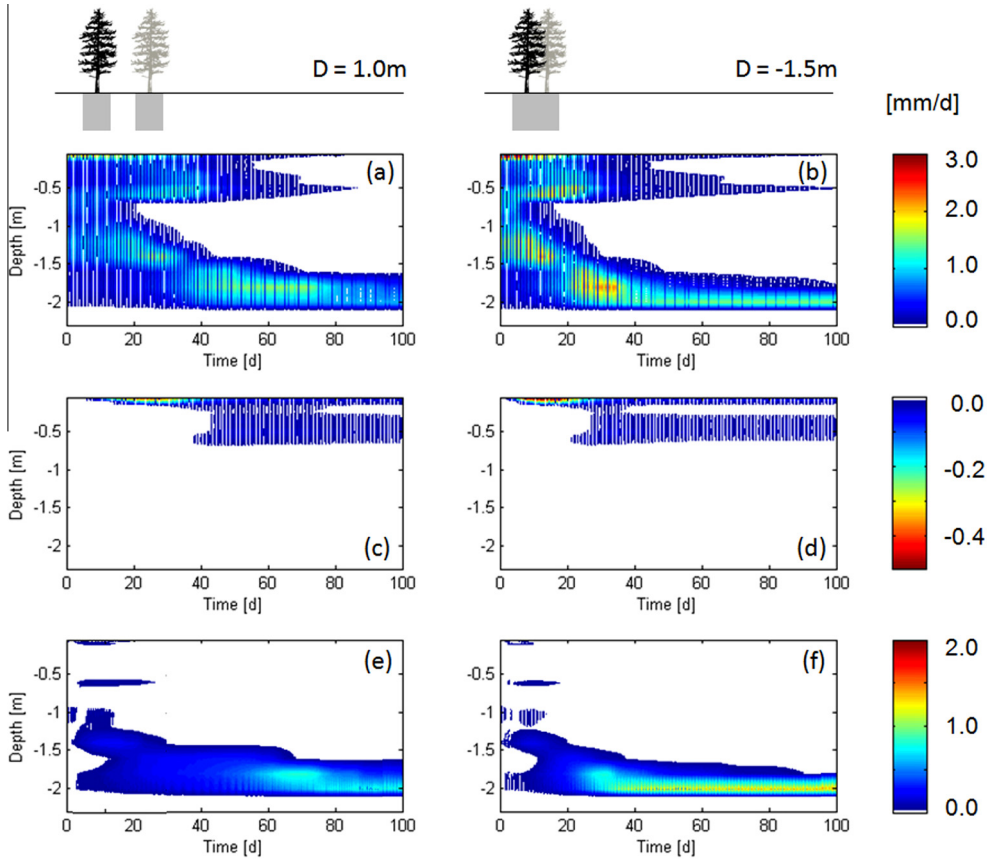

Fig. 7. Water fluxes in the root zone of tree T1: modeled (a, b) RWU, (c, d) HR and (e, f) the Darcy flux divergence as a function of depth for the case $D = 1$ m (left panels) and $D = -1.5$ m (right panels).

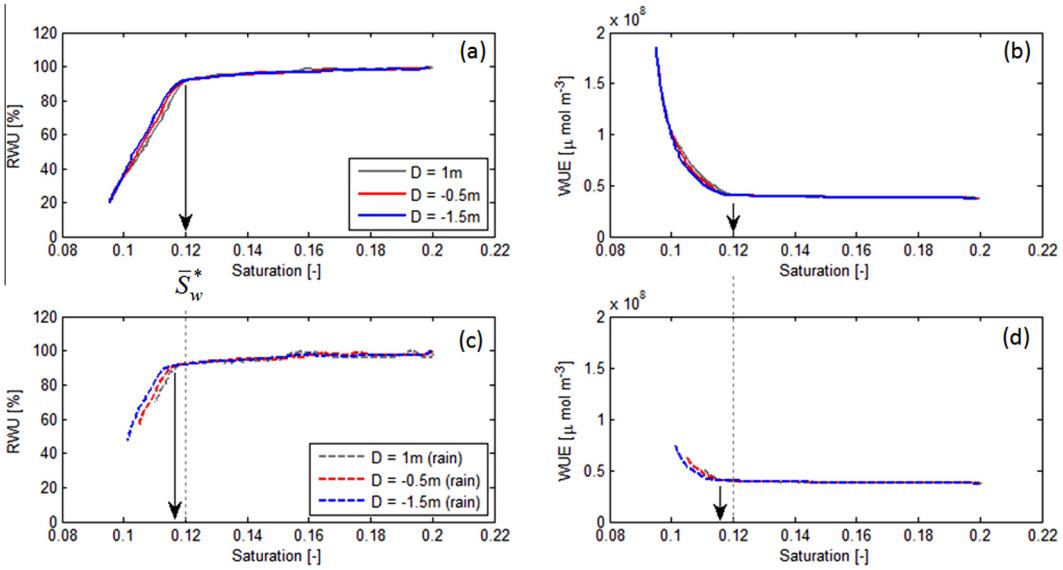

Fig. 8. Transpiration and soil saturation: (a, c) relative RWU and (b, d) WUE as a function of average soil saturation within the root zone during the drying cycle with (top panels) and without (bottom panels) rainfall.

often defined as a fraction of a maximum evapotranspiration for the ecosystem [46,47] through a water stress function, ρ, which varies with $\bar{S}_w : ET(\bar{S}_w) = \rho(\bar{S}_w) \cdot ET_{max}$. The form of $\rho(\bar{S}_w)$ and the value of ET_{max} are usually assumed with reference to a zeroth-dimensional spatial framework in which the effects of competition among rooting systems cannot be accounted for. The 3D nature of the model here is used to investigate the implications of root competition on the dependence of RWU/transpiration on $\bar{S}_w$. To this end, we extract from the dry-down experiments corresponding values of ET and $\bar{S}_w$ to construct $ET(\bar{S}_w)$ curves for different root spacings D (Fig. 8a). The relation between ET and soil-moisture appears insensitive to D and that

ET vs. $\rho(\bar{S}_w)$ curves collapse onto one another. That is, a unique function $\rho(\bar{S}_w)$ emerges even when tree spacing is altered (all else being the same). Irrespective of the D variations, hydraulic limitations to RWU commence when soil saturation drops below the same critical value of approximately $\bar{S}^*_w = 0.12$. Root competition speeds up the rate at which soil moisture stress is realized without actually altering the functional transpiration-soil moisture relation. The difference among root spacing scenarios lies in the speed at which the system traverses through the function in Fig. 8a. In particular, for $D = 1.0$ m (no overlap), $D = -0.5$ m, and $D = -1.5$ m, the critical soil moisture value is reached after 39, 29, and 24 days, respectively. The mean rainfall inter-arrival time at the site (see Supplementary material) is generally lower than the time needed for the system to reach such stress conditions (around 90% of the rainfall events has an inter-arrival time $\leqslant$8 days). However, inter-arrival times of 18 days have been observed in 2007–2008, and the degree of root overlapping may play an important role in controlling the transition to stress conditions. Interestingly, the decrease in RWU corresponds to an increase in the Water Use Efficiency (WUE), defined as the ratio of the whole plant photosynthetic rate to the plant transpiration rate (WUE $= f_c/f_w$), which is also insensitive to D (Fig. 8b). To verify the robustness of this insensitivity of the stress response function to root competition, further simulations with different boundary conditions were run. In particular, the effect of rainfall is evaluated by running drainage experiments in which a constant rainfall is applied at the top of the domain. An infiltration rate of 1 mm d^{-1} was assumed so as to explore how the modified vertical soil moisture profile impacts the $\rho(\bar{S}_w)$ form. Precipitation changes the soil moisture profile with respect to the simple drainage experiment by increasing the available water in the top soil (where most of the root biomass is) thus slowing down the onset of water stress. The main finding is that rainfall shifts the critical value of the mean soil moisture, $\bar{S}^*_w$, towards drier states (Fig. 8c and d). Furthermore, the shift of the critical value for water stress does exhibit a dependence on the amount of root overlap, albeit relatively mild. Comparable results are obtained from simulations with different soil properties (Supplementary material). These results suggest the existence of a stress response function that is independent of the degree of root overlap under dry conditions, but is dependent on rainfall amount and frequency and, mainly, on soil hydraulic properties. Understanding how the soil saturation-RWU relation varies under different hydrological conditions and root biomass allocation strategies is a topic for future work.

4.4. Limitations and perspectives

Interactions and competition among different rooting systems has been explored using a pine plantation as a case study. We assumed that the vertical root profiles of each tree in the plantation are identical and set to the observed root distribution in the simulations, constant in the lateral direction and time invariant. However, different adaptation strategies might be used by plants to optimally distribute biomass in the root zone [49] and these processes might become particularly relevant when the interaction between plants induces a rapid onset of water stress limiting their water use efficiency (as shown here). Even though these processes might not be dominant at large scales compared to other spatial processes (e.g., spatial variability of hydraulic properties, topography, root-zone spatial variation, multiple species, etc.…), they can become significant when tree scale processes are upscaled. Modeling these phenomena would require the incorporation of root dynamics and a detailed knowledge of root allocation strategies. Such work can build on the present results, but is outside the scope of this contribution.

5. Conclusions

A three-dimensional description of the soil–plant system is presented and applied to model root water uptake by overlapping rooting systems of Loblolly pine trees. The approach couples Richard's equation for soil moisture redistribution with a mechanistic description of plant transpiration and leaf photosynthesis. The results show that overlapping root systems affect soil moisture dynamics, Darcian redistribution, and hydraulic redistribution. When the three-dimensional RWU is volume-averaged in space, the main effect of overlapping root systems is to induce a more rapid onset of water stress conditions. Averaged ET vs. mean soil moisture relations are relatively independent of the degree of root overlap under dry conditions, but depend on soil hydraulic properties and, to a lesser extent, on the amount of rainfall infiltration. Because the model provides a 3D representation of the processes regulating root water uptake, it can be used to explore inherently spatial effects such as the role of soil heterogeneities and root allocation strategies on RWU and carbon uptake.

Acknowledgements

The authors acknowledge partial support from the University of Padova, Italy, within the Research Program "GEO-RISKS: Geological, morphological and hydrological processes: monitoring, modeling and impact in the north-eastern Italy", WP4. Additional support was provided by the US Department of Energy (DOE-BER) Terrestrial Ecosystem Sciences program (11-DE-SC-0006700 and DE-SC0006967), the US Department of Agriculture (USDA Grant 2011-67003-30222), the National Science Foundation (NSF-EAR-1344703 and NSF-AGS-1102227), the Binational Agricultural Research and Development Fund (IS-4374-11C), and the European Union – EU FP7 Collaborative Project CLIMB ("Climate Induced Changes on the Hydrology of Mediterranean Basins – Reducing Uncertainty and Quantifying Risk"). Support from the Nicholas School of the Environment and the Pratt School of Engineering (Duke University, Durham, NC, USA) is also acknowledged.

Appendix A. Supplementary data

Supplementary data associated with this article can be found, in the online version, at http://dx.doi.org/10.1016/j.advwatres.2014.01.006.

References

[1] Anderegg WRL, Kane JM, Anderegg LDL. Consequences of widespread tree mortality triggered by drought and temperature stress. Nature Clim Change 2013;3:30–6.
[2] Couvreur V, Vanderborght J, Javaux M. A simple three-dimensional macroscopic root water uptake model based on the hydraulic architecture approach. Hydrol Earth Syst Sci 2012;16:2957–71.
[3] Huxman TE, Wilcox BP, Breshears DD, Scott RL, Snyder KA, Small EE, Hultine K, Pockman WT, Jackson RB. Ecohydrological implications of woody plant encroachment. Ecology 2005;86:308–19.
[4] de Arellano JVG, van Heerwaarden CC, Lelieveld J. Modelled suppression of boundary-layer clouds by plants in a CO_2-rich atmosphere. Nature Geosci 2012;5:701–4.
[5] Maxwell RM, Chow FK, Kollet SJ. The groundwater–land–surface–atmosphere connection: soil moisture effects on the atmospheric boundary layer in fully-coupled simulations. Adv Water Resour 2007;30:2447–66.
[6] Dirmeyer PA, Koster RD, Guo Z. Do global models properly represent the feedback between land and atmosphere? J Hydrometeorol 2006;7:1177–98.
[7] Rodriguez-Iturbe I, D'Odorico P, Porporato A, Ridolfi L. Tree-grass coexistence in savannas: The role of spatial dynamics and climate fluctuations. Geophys Res Lett 1999;26:247–50.
[8] Richard JTV, Higgins SI, Bond WJ, E.C. (February). Water sourcing by trees in a mesic savanna: responses to severing deep and shallow roots. Environ Exp Bot 2011;74:229–36.

[9] Daly C, Bachelet D, Lenihan JM, Neilson RP, Parton W, Ojima D. Dynamic simulation of tree-grass interactions for global changes studies. Ecol Appl 2000;10:449–69.
[10] Feddes R, Kowalik P, Zaradny H. Simulation on of field water use and crop yield, Technical Report. Wageningen, the Netherlands: Centre for Agricultural Publishing and Documentation; 1978.
[11] Jarvis NJ. The MACRO model (Version 3.1), technical description and sample simulations. Reports and Dissertations 19, Technical Report, Dep. Soil Sci., Swedish Univ. Agric. Sci, Uppsala, Sweden, 1994.
[12] Šimůnek J, van Genuchten MT, Šejna M. The HYDRUS Software Package for Simulating the Two- and Three-Dimensional Movement of Water, Heat, and Multiple Solutes in Variably-Saturated Media. Technical Report, PC-Progress, Prague, Czech Republic, March 2006.
[13] Vogel T, Dohnal M, Dusek J, Votrubova J, Tesar M. Macroscopic modeling of plant water uptake in a forest stand involving root-mediated soil water redistribution. Vadose Zone J 2013;12.
[14] Caldwell MM, Richards JH. Hydraulic lift: Water efflux from upper roots improves effectiveness of water uptake by deep roots. Oecologia 1989;79:1–5.
[15] Domec JC, King JS, Noormets A, Treasure E, Gavazzi MJ, Sun G, McNulty SG. Hydraulic redistribution of soil water by roots affects whole-stand evapotranspiration and net ecosystem carbon exchange. New Phytol 2010;187:171–83.
[16] Mendel M, Hergarten S, Neugebauer HJ. On a better understanding of hydraulic lift: a numerical study. Water Resour Res 2002;38:1183.
[17] Siqueira M, Katul G, Porporato A. Onset of water stress, hysteresis in plant conductance, and hydraulic lift: Scaling soil water dynamics from millimeters to meters. Water Resour Res 2008;44:WR01432.
[18] Amenu GG, Kumar P. A model for hydraulic redistribution incorporating coupled soil-root moisture transport. Hydrol Earth Syst Sci 2008;12:55–74.
[19] Siqueira M, Katul G, Porporato A. Soil moisture feedbacks on convection triggers: the role of soil–plant hydrodynamics. J Hydrometeorol 2009;10:96–112.
[20] Domec JC, Ogée J, Noormets A, Jouangy J, Gavazzi MJ, Treasure E, Sun G, McNulty SG, King JS. Interactive effects of nocturnal transpiration and climate change on the root hydraulic redistribution and carbon and water budgets of southern United States pine plantations. Tree Phys 2012;32:707–23.
[21] Neumann RB, Cardon ZG. The magnitude of hydraulic redistribution by plant roots: a review and synthesis of empirical and modeling studies. New Phytol 2012;194:337–52.
[22] Volpe V, Marani M, Albertson JD, Katul G. Root controls on water redistribution and carbon uptake in the soil–plant system under current and future climate. Adv Water Resour 2013;60:110–20.
[23] Ivanov VY, Bras RL, Vivoni ER. Vegetation-hydrology dynamics in complex terrain of semiarid areas: 1. A mechanistic approach to modeling dynamic feedbacks. Water Resour Res 2008;44:W03429.
[24] Kuhlmann A, Neuweiler I, van der Zee SEATM, Helmig R. Influence of soil structure and root water uptake strategy on unsaturated flow in heterogeneous media. Water Resour Res 2012;48:W02534.
[25] Javaux M, Schröder T, Vanderborght J, Vereecken H. Use of a three-dimensional detailed modeling approach for predicting root water uptake. Vadose Zone J 2008;7:1079–88.
[26] Doussan C, Pierret A, Garrigues E, Pages L. Water uptake by plant roots: II – Modelling of water transfer in the soil rootsystem with explicit account of flow within the root system – Comparison with experiments. Plant Soil 2006;283:99–117.
[27] Kalbacher T, Schneider CL, Wang W, Hildebrandt A, Attinger S, Kolditz O. Modeling soil-coupled water uptake of multiple root system with automatic time stepping. Vadose Zone J 2011;10:727–35.
[28] van Genuchten MT, Nielsen DR. On describing and predicting the hydraulic properties of unsaturated soils. Ann Geophys 1985;3:615–28.
[29] Camporese M, Paniconi C, Putti M, Orlandini S. Surface-subsurface flow modeling with path-based runoff routing, boundary condition-based coupling, and assimilation of multisource observation data. Water Resour Res 2010;46:W02512.
[30] Paniconi C, Putti M. A comparison of Picard and Newton iteration in the numerical-solution of multidimensional variably saturated flow problems. Water Resour Res 1994;30:3357–74.
[31] Bergamaschi L, Bru R, Martinez A, Putti M. Quasi-newton preconditioners for the inexact Newton method. Electron Trans Numer Anal 2006;23:76–87.
[32] Bergamaschi L, Bru R, Martinez A, Mas J, Putti M. Low-rank update of preconditioners for the nonlinear Richards equation. Math Comput Model 2013;57:1933–41.
[33] de Willigen P, van Noordwijk M. Roots, plant production, and nutrient use efficiency, Ph.D. thesis, Agricultural Univ. Wageningen, The Netherlands, 1987.
[34] Daly E, Porporato A, Rodriguez-Iturbe I. Coupled dynamics of photosynthesis, transpiration, and soil water balance. Part I: Upscaling from hourly to daily level. J Hydrometeorol 2004;5:546–58.
[35] Farquhar GD, von Caemmerer S, Berry JA. A biochemical model of photosynthetic CO_2 assimilation in leaves of C_3 species. Planta 1980;149:78–90.
[36] Campbell GS, Norman JM. An Introduction to Environmental Biophysics. New York: Springer; 2000.
[37] Katul G, Manzoni S, Palmroth S, Oren R. A stomatal optimization theory to describe the effects of atmospheric CO_2 on leaf photosynthesis and transpiration. Ann Botany 2010;105:431–42.
[38] Novick K, Oren R, Stoy P, Siqueira M, Katul GG. Nocturnal evapotranspiration in eddy-covariance records from three co-located ecosystems in the Southeastern US: Implications for annual fluxes. Agr Forest Meteorol 2009;149:1491–504.
[39] Manzoni S, Vico G, Katul P, Fay G, Polley W, Palmroth S, et al. Optimizing stomatal conductance for maximum carbon gain under water stress: a meta-analysis across plant functional types and climates. Funct Ecol 2011;25:456–67.
[40] Sun G, Noormets A, Gavazzi MJ, McNulty SG, Chen J, Domec JC, King JS, Amatya DM, Skaggs RW. Energy and water balance of two contrasting loblolly pine plantations on the lower coastal plain of North Carolina, USA. Forest Ecol Manag 2010;259:1299–310.
[41] Diggs J. Hydrology and nitrogen loading of forested fields in a coastal plain watershed. Master's thesis, North Carolina State University, Raleigh, NC, USA, 2004.
[42] Aspinwall MJ, King JS, Domec JC, McKeand SE, Isik F. Genetic effects on transpiration, canopy conductance, stomatal sensitivity to vapour pressure deficit, and cavitation resistance in loblolly pine. Ecohydrology 2011;4:168–82.
[43] Samuelson L, Stokes T, Cooksey T, McLemore Pt. Production efficiency of loblolly pine and sweetgum in response to four years of intensive management. Tree Phys 2001;21:369–76.
[44] Eagleson PS. Climate, soil and vegetation. 1. Introduction to water balance dynamics. Water Resour Res 1978;14:705–12.
[45] Milly PCD. An analytical solution of the stochastic storage problem applicable to soil water. Water Resour Res 1993;29:3755–8.
[46] Rodriguez-Iturbe I, Porporato A, Ridolfi L, Isham V, Cox D. Probabilistic modelling of water balance at a point: the role of climate, soil and vegetation. Proc R Soc Lond A 1999;455:3789–805.
[47] Laio F, Porporato A, Ridolfi L, Rodriguez-Iturbe I. Plants in water-controlled ecosystems: active role in hydrologic processes and response to water stress. II. Probabilistic soil moisture dynamics. Adv Water Resour 2001;24:707–23.
[48] Porporato A, Daly E, Rodriguez-Iturbe I. Soil water balance and ecosystem response to climate change. Am Nat 2004;164:625–32.
[49] Ho MD, McCannon BC, Lynch JP. Optimization modeling of plant root architecture for water and phosphorus acquisition. J Theor Biol 2004;226:331–4.